Analysis on Tidal Inlet Stability

Leo Guo

Delft University of Technology
BSc Applied Mathematics | BSc Applied Physics
Bachelor's Thesis

Supervision committee:
H.M. Schuttelaars
S.R. de Roode
F. Bociort
M.C. Veraar
J.A.M. de Groot

Abstract

The main goal of this project is to predict the influence of non-uniform basin depths on the stability of single inlet systems. This is achieved by making use of Escoffier's principle, which poses a relationship between the relative water flow velocity in an inlet and the rate of change of its cross-sectional area. To this end, a thorough analysis is performed on the equations that govern water motions, principially the linearised shallow water equations. An analytic solution is obtained, and some results are simulated in MATLAB.

Contents

1 Introduction

Chains of barrier islands are a common occurence along coastlines around the world. In general, a barrier island chain consists of a *basin*, usually relatively shallow, which is separated from the rest of the sea or ocean to which it is attached. This separation comprises one or more *inlet channels*, linking the basin to the outer sea. When multiple inlet channels are involved, barrier islands will be existing inbetween the channels.
In the Netherlands, the *Waddeneilanden* along with the inlets that separate them form such a barrier coast. The chain of islands stretches up to a length of 500 km between the Netherlands and Denmark [8].

Figure 1: Satellite image of the Waddeneilanden. *Google Maps* (2016)

Although the islands themselves are quite small, approximately 1000 km^2, they enclose a rather sizable area of inland sea called the *Wadden Sea*. This marginal sea spans a maximal area of about 10 000 km^2 during high tide, of which approximately 75% runs dry partially or entirely during low tide [7].
As one might imagine, this kind of environment has the ability to house flora and fauna that is unique to the Wadden region. In fact, a large portion of the islands and the Wadden Sea have been declared as a UNESCO World Heritage in 2009 [9].
Not only is nature a significant aspect of this region, but these islands also possess cultural importance. Although the shapes of the islands were quite different in the past, records show that this region has been inhabited for over 2000 years. Nowadays, a population of approximately 80 000 people reside permanently on the islands, whereas a lot more people

stay on the islands during summer when the islands form a tourist hotspot [8].
Arising from its ecological and economic importance, it is desirable to know how the island chain changes its shape over long periods of time. The islands are subject to continuous changes due to sediment transport by sea currents. As a result, numerous villages have disappeared in the past as they were engulfed by the sea.
To know how water flow changes island shapes is important to our understanding of geological phenomena. In what fashion and shape do tidal flats, similar to the ones in the Wadden Sea, as can be seen in Figure 1, come to be? A similar formulation of this question would be: how does water flow through inlet channels affect them over time?

In this thesis, all physical quantities and equations that relate to each other which are deemed to be important, will be analysed. In addition to physical parameters, the geometries in which these phenomena take place will be considered and discussed. This is mainly done in chapter 2, where the single-inlet system is introduced as the main geometry of interest; chapter 3 is devoted to analysing the equations and introducing techniques that solve the equations, and chapter 4 contains some basic results of the findings. During the final chapter, some further research potentials will be highlighted that are beyond the scope of this thesis.

2 Parameters and Models

2.1 Geometries

In this chapter, one will see the definitions of some physical quantities and measures [1]. These are related to the geometry that will be introduced to analyse the inlet stability: the single-inlet system, depicted in Figure 2.

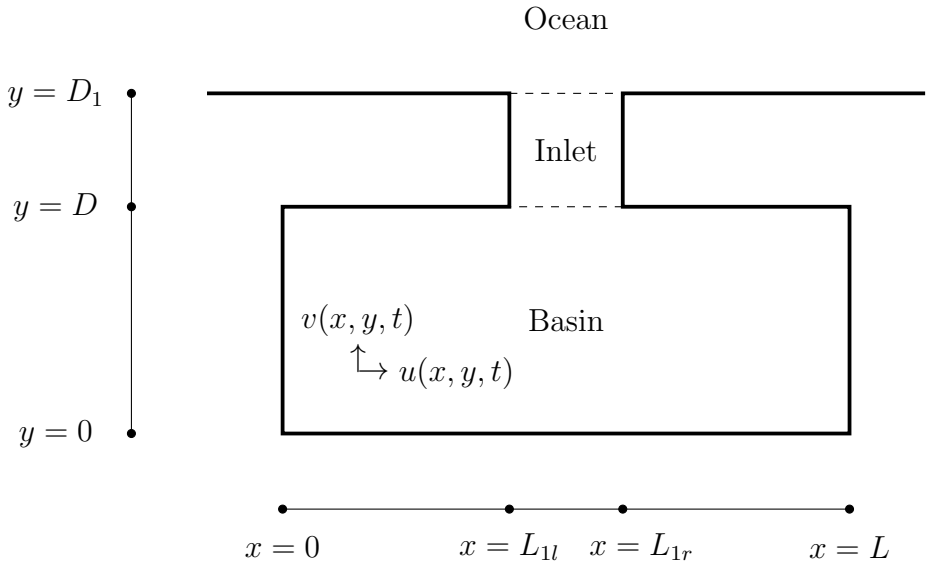

Figure 2: Top view of a single-inlet system.

From the figure, all coordinates of this two-dimensional system can be seen. The inlet system consists of three different bodies of water that are connected to each other. The basin is attached to the inlet channel at one side, and the other end of the inlet is attached to the ocean. The basin and inlet are both considered to have a rectangular top view, with dimensions $L \times D$ and $\Delta L_1 \times \Delta D$ respectively, where $\Delta L_1 := L_{1r} - L_{1l}$ and $\Delta D := D_1 - D$. The relative dimensions of the ocean are considered large enough to be modeled as semi-infinite. Two water flow velocities are defined, that depend on the spatial variables x and y, but also on time t. One defines $u(x, y, t)$ to be the velocity in the x-direction, while $v(x, y, t)$ is the velocity in the y-direction.

[1] A list containing the numerical values of physical quantities used throughout this thesis can be found in the Appendix.

In addition to the top view of the single-inlet system, a cross-section of the basin will be taken to define the water depth $H(x, y)$ and the sea level perturbation $\zeta(x, y, t)$.

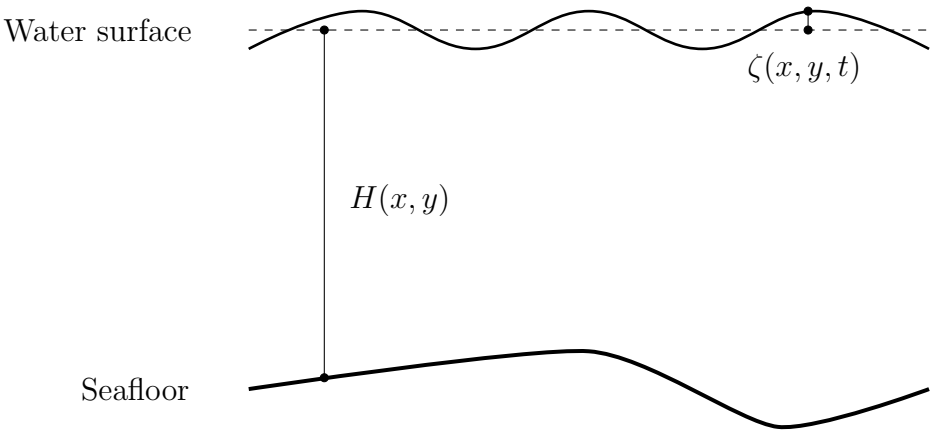

Figure 3: Part of the basin's cross-sectional area.

The dashed line segment in Figure 2.1 indicates the mean sea level, which can be chosen to be 0. Note that ζ is measured postively upwards, while H is measured positively downwards. These quantities are defined in a similar way when the inlet channel is concerned.

During previous researches (see e.g. [1], [2]), the basin water depth H is assumed to be constant. In this thesis, one will carry out the analyses while assuming that the basin water depth exhibits space-dependent variations.

2.2 Escoffier's Principle and the Shallow Water Equations

In order to formulate a general idea of the main problem that will be of concern in this thesis, Escoffier's principle will now be introduced:

$$\frac{\mathrm{d}A}{\mathrm{d}t} = \frac{\mu}{\Delta D}\left[\left(\frac{U}{U_{\mathrm{eq}}}\right)^{\kappa} - 1\right]. \tag{2.2.1}$$

Given an inlet that connects the basin to the ocean, this equation gives the relation between an inlet's cross-sectional area A and the cross-sectionally averaged flow speed U throughout the inlet, relative to U_{eq}, which is defined as an equilibrium flow speed. Indeed, if $U = U_{\mathrm{eq}}$, then $\frac{\mathrm{d}A}{\mathrm{d}t} = 0$, which means that the cross-sectional area of the inlet does not change over time: it has reached an equilibrium. On the other hand, if $U < U_{\mathrm{eq}}$ or $U > U_{\mathrm{eq}}$, then A will respectively decrease and increase.
In Escoffier's equation, the sedimental composition related parameters μ and κ also play a role; μ is the sediment import by the process of ebb and flow, and κ is the power that is related to the power law of sediment transport.
The quantity U is defined as

$$U = \frac{1}{\Delta L_1 \cdot \Delta D}\iint_R |u|\,\mathrm{d}(x, y) \tag{2.2.2}$$

where R is the inlet region with dimensions $\Delta L_1 \times (D_1 - D)$. Note that if one defines the width of the inlet channel as

$$\Delta L_1 = \frac{A}{H^{\mathrm{I}}} \tag{2.2.3}$$

where H^{I} is the water depth in the inlet, then U depends on A according to (2.2.2). Subsequentially, if u has been solved for, then A can be calculated for future time by e.g. using a numerical integration scheme [1].

In order to use (2.2.1) and (2.2.2), it is important to calculate the water flow velocity in the single inlet system. Water motions are governed by the conservation of mass and momentum. Mathematically, this is described by the *Navier-Stokes equation*. Given the numerical parameters in the Appendix, it is reasonable to assume that all concerned water depths in the specified geometry of Figure 2.1 ($\sim$10m) are small with respect to the horizontal length scales ($\sim$10km). Then, by depth-integrating the Navier-Stokes equation, the *linearized shallow water equations* can be derived. For more details on the analysis, refer to [4].

$$\frac{\partial u}{\partial t} - fv(x,y) + \frac{r}{H(x,y)}u(x,y) = -g\frac{\partial \zeta}{\partial x}, \tag{2.2.4}$$

$$\frac{\partial v}{\partial t} + fu(x,y) + \frac{r}{H(x,y)}v(x,y) = -g\frac{\partial \zeta}{\partial y}, \tag{2.2.5}$$

$$\frac{\partial \zeta}{\partial t} + \frac{\partial}{\partial x}[H(x,y)u(x,y)] + \frac{\partial}{\partial y}[H(x,y)v(x,y)] = 0. \tag{2.2.6}$$

These equations in two spatial parameters x and y and time t pose a relationship between the depth-averaged x- and y-directional water flow, $u(x,y)$ and $v(x,y)$ respectively, as well as the sea level perturbation $\zeta(x,y)$ for every position (x,y) in the concerned region.
f is the Coriolis parameter, and is defined as

$$f = 2\Omega \sin(\theta), \tag{2.2.7}$$

where $\Omega = 7.292 \cdot 10^{-5}$ rad s^{-1} is the angular frequency of Earth's rotation and θ is the central latitude of the basin-inlet system. r is the bottom friction coefficient throughout the system, and g is the local gravitational acceleration.

3 Equation Analyses

3.1 Isolated Basin with Constant Basin Depth

As for a first analysis on how the shallow water equations are solved, one will consider a rectangular basin with dimensions $L \times D$ that is subject to no external boundary forces.

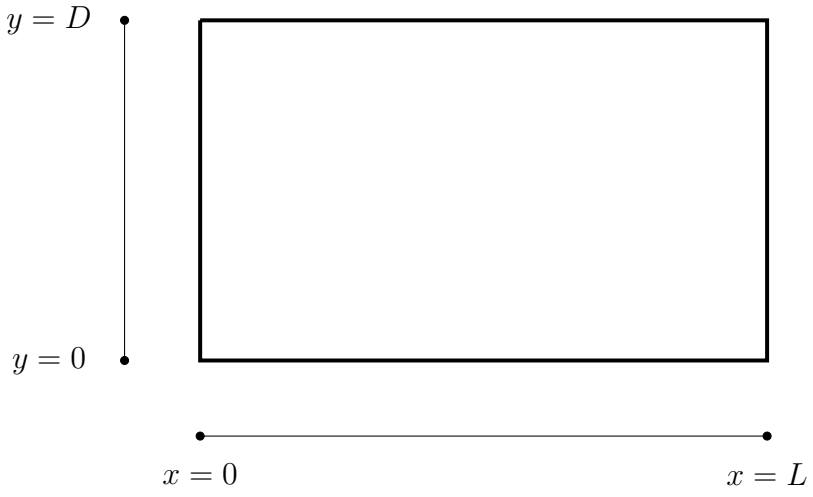

Figure 4: An isolated rectangular basin.

The basin depth $H(x, y) = H$ is assumed constant. Equation (2.2.6) now reduces to a simpler form:

$$\frac{\partial \zeta}{\partial t} + H\left(\frac{\partial u}{\partial x} + \frac{\partial v}{\partial y}\right) = 0. \tag{3.1.1}$$

Next, define the operator

$$\mathcal{L} := \frac{\partial}{\partial t} + \frac{r}{H}. \tag{3.1.2}$$

Equations (2.2.4) and (2.2.5) can then be rewritten as

$$\mathcal{L}u - fv = -g\frac{\partial \zeta}{\partial x}, \tag{3.1.3}$$

$$\mathcal{L}v + fu = -g\frac{\partial \zeta}{\partial y}. \tag{3.1.4}$$

Let $\mathcal{L}$ act on (3.1.3) and multiply f with (3.1.4). By adding the results, one will find a direct relation between the flow velocity u and sea level ζ.

$$(\mathcal{L}^2 + f^2)u = -g\left(\mathcal{L}\frac{\partial \zeta}{\partial x} + f\frac{\partial \zeta}{\partial y}\right) \tag{3.1.5}$$

By letting $\mathcal{L}$ act on (3.1.4) and multiplying f with (3.1.3), and subsequentially taking the difference between the results, v and ζ are related by

$$(\mathcal{L}^2 + f^2)v = -g\left(\mathcal{L}\frac{\partial \zeta}{\partial y} - f\frac{\partial \zeta}{\partial x}\right) \tag{3.1.6}$$

Next, by letting $\mathcal{L}^2 + f^2$ act on (3.1.1), one will find

$$(\mathcal{L}^2 + f^2)\frac{\partial \zeta}{\partial t} + H\left(\frac{\partial}{\partial x}(\mathcal{L}^2 + f^2)u + \frac{\partial}{\partial y}(\mathcal{L}^2 + f^2)v\right) = 0. \tag{3.1.7}$$

Using equations (3.1.5) and (3.1.6), it follows that

$$\frac{\partial}{\partial x}(\mathcal{L}^2 + f^2)u = -g\left(\mathcal{L}\frac{\partial^2 \zeta}{\partial x^2} + f\frac{\partial^2 \zeta}{\partial x \partial y}\right); \quad \frac{\partial}{\partial y}(\mathcal{L}^2 + f^2)v = -g\left(\mathcal{L}\frac{\partial^2 \zeta}{\partial y^2} - f\frac{\partial^2 \zeta}{\partial x \partial y}\right).$$

With this information, equation (3.1.7) can be written as

$$(\mathcal{L}^2 + f^2)\frac{\partial \zeta}{\partial t} + H\left[-g\left(\mathcal{L}\frac{\partial^2 \zeta}{\partial x^2} + f\frac{\partial^2 \zeta}{\partial x \partial y}\right) - g\left(\mathcal{L}\frac{\partial^2 \zeta}{\partial y^2} - f\frac{\partial^2 \zeta}{\partial x \partial y}\right)\right] = 0,$$

which is equivalent to

$$(\mathcal{L}^2 + f^2)\frac{\partial \zeta}{\partial t} - gH\mathcal{L}\left(\frac{\partial^2 \zeta}{\partial x^2} + \frac{\partial^2 \zeta}{\partial y^2}\right) = 0. \tag{3.1.8}$$

Hence, to solve the system of shallow water equations, one can first solve for ζ by using (3.1.8), and once the solution is known, u and v can be determined by solving (3.1.5) and (3.1.6) respectively. In order to solve for non-trivial ζ, the standard procedure of separation of variables can be used by noting that $\mathcal{L}$ is a linear differential operator and by assuming $\zeta(x, y, t) = X(x)Y(y)T(t)$ [3]. The following ODEs arise:

$$(\mathcal{L}^2 + f^2)\frac{\mathrm{d}T}{\mathrm{d}t} = -\lambda\mathcal{L}(T), \tag{3.1.9}$$

$$\frac{\mathrm{d}^2 X}{\mathrm{d}x^2} = -\mu X, \tag{3.1.10}$$

$$\frac{\mathrm{d}^2 Y}{\mathrm{d}y^2} = -\left(\frac{\lambda}{gH} - \mu\right)Y. \tag{3.1.11}$$

Boundary conditions will be needed to solve for X and Y. At the boundaries, the flow velocities should vanish.

$$u(0, y, t) = u(L, y, t) = v(x, 0, t) = v(x, D, t) = 0 \tag{3.1.12}$$

According to (3.1.5) and (3.1.6), these conditions are equivalent to

$$\mathcal{L}(T)Y\frac{\mathrm{d}X}{\mathrm{d}x} + fXT\frac{\mathrm{d}Y}{\mathrm{d}y} = 0, \quad \mathcal{L}(T)X\frac{\mathrm{d}Y}{\mathrm{d}y} - fYT\frac{\mathrm{d}X}{\mathrm{d}x} = 0. \tag{3.1.13}$$

To simplify these mixed boundary conditions somewhat, the Coriolis parameter will be henceforth considered negligible ($f \approx 0$) for this case, i.e.: force terms due to the rotation of the Earth are neglected. Since $X, Y \neq 0$ as only non-trivial solutions are relevant as well as $\mathcal{L}(T) \neq 0$ [2], all boundary conditions for X and Y reduce to the Neumann type.

$$\frac{\mathrm{d}X}{\mathrm{d}x}(0) = \frac{\mathrm{d}X}{\mathrm{d}x}(L) = \frac{\mathrm{d}Y}{\mathrm{d}y}(0) = \frac{\mathrm{d}Y}{\mathrm{d}y}(D) = 0. \tag{3.1.14}$$

[2] If this were the case, $\frac{\mathrm{d}T}{\mathrm{d}t} = 0$, which means that the solution is stationary, hence trivial by choice.

The corresponding boundary conditions for ζ are indicated in Figure 5.

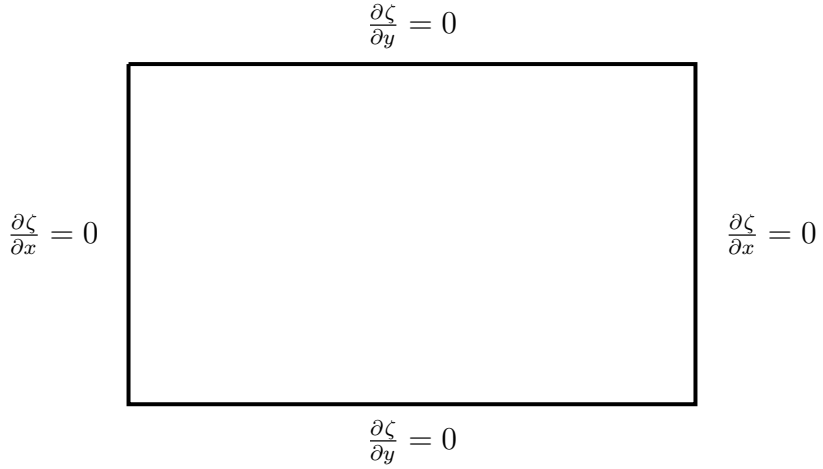

Figure 5: Isolated basin with indicated boundary conditions for ζ.

Standard techniques show that the labeled eigenfunctions satisfying (3.1.10) and (3.1.11) are

$$X_n(x) = \cos\left(\frac{n\pi x}{L}\right), \quad Y_m(y) = \cos\left(\frac{m\pi y}{D}\right) \tag{3.1.15}$$

with the usual eigenvalues

$$\lambda_{nm} = gH\left[\left(\frac{n\pi}{L}\right)^2 + \left(\frac{m\pi}{D}\right)^2\right]. \tag{3.1.16}$$

By the principle of superposition of solutions, the general ζ is thus given by

$$\zeta(x, y, t) = \sum_{n=0}^{\infty}\sum_{m=0}^{\infty} a_{nm} \cos\left(\frac{n\pi x}{L}\right)\cos\left(\frac{m\pi y}{D}\right) T_{nm}(t). \tag{3.1.17}$$

Now (3.1.10) and (3.1.11) have been solved for, it remains to solve (3.1.9), which is a third order linear ordinary differential equation. Note that

$$\mathcal{L}^2 = \frac{\mathrm{d}^2}{\mathrm{d}t^2} + 2\frac{r}{H}\frac{\mathrm{d}}{\mathrm{d}t} + \left(\frac{r}{H}\right)^2,$$

such that the characteristic equation for (3.1.9) generated by the trial function $T(t) = e^{\alpha_{nm}t}$ becomes

$$\alpha_{nm}^3 + 2\frac{r}{H}\alpha_{nm}^2 + \left[\left(\frac{r}{H}\right)^2 + \lambda_{nm}\right]\alpha_{nm} + \frac{r}{H}\lambda_{mn} = 0. \tag{3.1.18}$$

The three complex α_{nm} that are able to solve this third order equation can be written in a closed-form expression, but a quick numerical simulation shows that for every $m, n \neq 0$, the real part of α_{nm} is negative. This means that $\lim_{t\to\infty} T_{nm}(t) = 0$, and by extension,

$\lim_{t\to\infty} \zeta(x, y, t) = 0$ by contribution from every of its nonzero modes.

When $m = n = 0$, it can be easily seen that $\alpha = 0$ is a solution to (3.1.18). This corresponds to the constant mode in (3.1.17), which means that it is the unique mode that does not dissipate over time. It turns out that one can choose the amplitude of this mode to equal zero, as all boundary conditions are of the Neumann type. That is: in all cases, not ζ itself is prescribed, but one of its partial derivatives. This leaves one order of freedom in choice for the constant term: one is essentially free to choose its level of zero potential gravitational energy on any height. This holds regardless of whether the basin bathymetry is constant, as H can be defined as the mean water depth in the basin. For all the other modes, it is rather obvious that disturbances in the water level disappear over time, as it is stipulated that $r > 0$; there is nonzero friction, which dissipates the kinetic energy of the water in the isolated basin.

3.2 Basin Attached to the Ocean

Now that solutions for ζ have been established to damp out in isolated basins, it is reasonable to assume that the water in the basin adopts any long-term behaviour of external water forces. To this end, another basin geometry will be introduced on which the shallow water equations will be analysed.

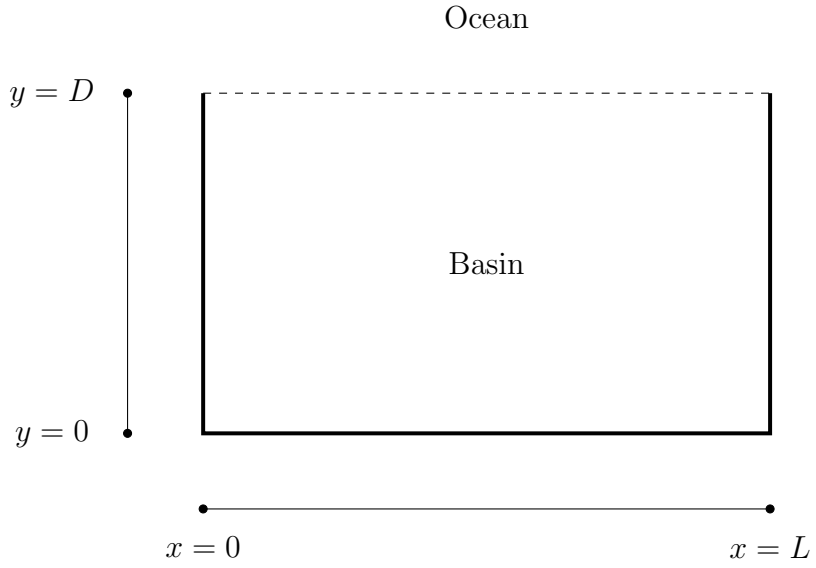

Figure 6: A non-isolated rectangular basin.

Figure 6 shows that the geometry is relatively similar to the one discussed in the previous paragraph. At $y = D$, the basin is connected to the ocean, which will be able to exert periodic forcing of the basin water by means of ebb and flow. This gives rise to the following:

$$\{u, v, \zeta\} = \mathrm{Re}\left[\{\tilde{u}, \tilde{v}, \tilde{\zeta}\}e^{-i\omega t}\right]. \tag{3.2.1}$$

As it turns out, by introducing this periodic time dependency of the flow velocities and sea level in the basin, $\tilde{u}(x,y)$, $\tilde{v}(x,y)$ and $\tilde{\zeta}(x,y)$ can be analysed in detail.
By substituting the proposed solution forms in (3.2.1) into the shallow water equations (2.2.4) through (2.2.6), all time dependencies can be canceled out because the equations are linear. By yet ignoring the Coriolis forces in favor of nicer boundary conditions, the new system of time-independent shallow water equations reads:

$$-i\omega\tilde{u} + \frac{r}{H}\tilde{u} = -g\frac{\partial\tilde{\zeta}}{\partial x}, \tag{3.2.2}$$

$$-i\omega\tilde{v} + \frac{r}{H}\tilde{v} = -g\frac{\partial\tilde{\zeta}}{\partial y}, \tag{3.2.3}$$

$$-i\omega\tilde{\zeta} + \frac{\partial}{\partial x}(H\tilde{u}) + \frac{\partial}{\partial y}(H\tilde{v}) = 0. \tag{3.2.4}$$

This system involves only two independent variables, as opposed to three in the original shallow water equations. These equations will now be analysed with topographic variations in consideration, i.e. $H(x,y)$ is non-constant.
As with the time-dependent shallow water system, where the operator $\mathcal{L}$ was defined, one can analogously define the scalar quantity

$$M(x,y) = -i\omega + \frac{r}{H(x,y)} \tag{3.2.5}$$

which fulfills the same role in the time-independent system, equations (3.2.2) through (3.2.4). Equations (3.2.2) and (3.2.3) can be rewritten to obtain direct relations between $\tilde{u}$, $\tilde{v}$ and $\tilde{\zeta}$.

$$\tilde{u} = -\frac{g}{M}\frac{\partial\tilde{\zeta}}{\partial x}, \tag{3.2.6}$$

$$\tilde{v} = -\frac{g}{M}\frac{\partial\tilde{\zeta}}{\partial y}. \tag{3.2.7}$$

These expressions can be directly substituted into (3.2.4) to find

$$\tilde{\zeta} - \frac{\partial}{\partial x}\left(\frac{gHi}{\omega M}\frac{\partial\tilde{\zeta}}{\partial x}\right) - \frac{\partial}{\partial y}\left(\frac{gHi}{\omega M}\frac{\partial\tilde{\zeta}}{\partial y}\right) = 0. \tag{3.2.8}$$

There are different methods that can be used to solve (3.2.8). This can be done by applying an iterative numerical scheme [5], but the rest of this paragraph will be devoted to deriving and analysing an analytical approach.
To this end, perturbation theory will be applied to investigate the influence of small bathymetry perturbations on the water motion in the basin. $H(x,y)$ will be written as

$$H(x,y) = H_0 + \delta h(x,y) \tag{3.2.9}$$

for some constant H_0 and a continuous function $h(x,y)$, and δ being a small parameter. Using this, one can expand $1/H$ geometrically.

$$\frac{1}{H} = \frac{1}{H_0(1+\frac{h}{H_0}\delta)} = \frac{1}{H_0}\sum_{k=0}^{\infty}(-1)^k\left(\frac{h}{H_0}\right)^k\delta^k. \tag{3.2.10}$$

Then, $1/M$ is also expanded geometrically:

$$\frac{1}{M} = \frac{1}{\frac{r}{H} - i\omega} = \frac{i}{\omega} \sum_{n=0}^{\infty} \left[\frac{r}{i\omega H_0} \sum_{k=0}^{\infty} (-1)^k \left(\frac{h}{H_0} \right)^k \delta^k \right]^n. \tag{3.2.11}$$

Next, the sea level ζ is expanded in the small paramater δ as well,

$$\zeta(x, y) = \sum_{n=0}^{\infty} \zeta_n(x, y)\delta^n. \tag{3.2.12}$$

By substituting all expansions into (3.2.8), one finds

$$\begin{aligned} \sum_{n=0}^{\infty} \tilde{\zeta}_n(x, y)\delta^n - \frac{\partial}{\partial x} \left(-\frac{g}{\omega^2}(H_0 + \delta h) \sum_{n=0}^{\infty} \left[\frac{r}{i\omega H_0} \sum_{k=0}^{\infty} (-1)^k \left(\frac{h}{H_0} \right)^k \delta^k \right]^n \sum_{n=0}^{\infty} \frac{\partial \tilde{\zeta}_n}{\partial x} \delta^n \right) \\ - \frac{\partial}{\partial y} \left(-\frac{g}{\omega^2}(H_0 + \delta h) \sum_{n=0}^{\infty} \left[\frac{r}{i\omega H_0} \sum_{k=0}^{\infty} (-1)^k \left(\frac{h}{H_0} \right)^k \delta^k \right]^n \sum_{n=0}^{\infty} \frac{\partial \tilde{\zeta}_n}{\partial y} \delta^n \right) = 0. \end{aligned} \tag{3.2.13}$$

This equation shows that for every order in δ, the terms with the same order in δ must balance. With this in mind, gathering the 0th order (constant) δ terms yields the following equation:

$$\tilde{\zeta}_0 - \frac{gH_0 i}{\omega M_0} \left(\frac{\partial^2 \tilde{\zeta}_0}{\partial x^2} + \frac{\partial^2 \tilde{\zeta}_0}{\partial y^2} \right) = 0. \tag{3.2.14}$$

One may recognise (3.2.14) as a homogeneous Helmholtz equation. Define

$$\tilde{k}^2 = \frac{\omega M_0 i}{gH_0} \tag{3.2.15}$$

such that

$$\nabla^2 \tilde{\zeta}_0 + \tilde{k}^2 \tilde{\zeta}_0 = 0. \tag{3.2.16}$$

This PDE can be solved in a relatively straightforward fashion on the given geometry by considering its boundary conditions. In this case, the problem concerns the rectangular region shown in Figure 6, which has three sides with Neumann boundaries. The remaining side is connected with the ocean, which will now be simulated by a prescribed flow velocity boundary, namely $\frac{\partial \tilde{\zeta}_0}{\partial y}(x, D) = z(x)$.

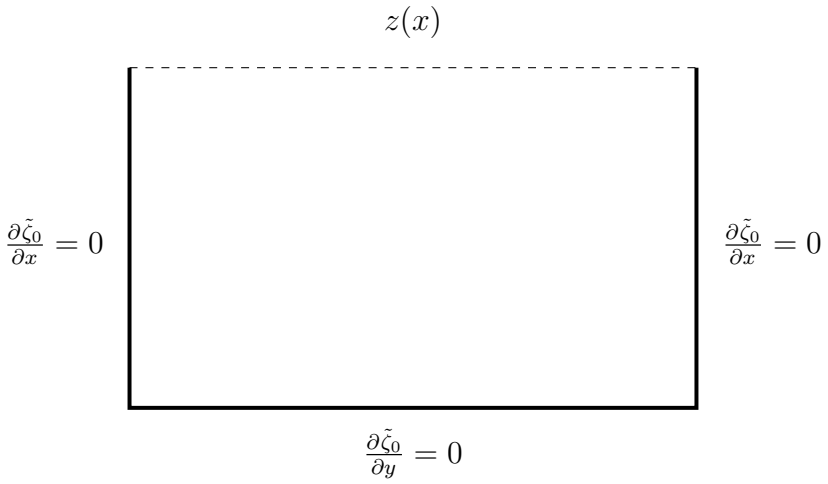

Figure 7: The same basin as in Figure 6, with indicated boundary conditions.

Given these boundary conditions, the general solution for $\tilde{\zeta}_0$ can be obtained through standard techniques. Define

$$\lambda_n = \sqrt{\left(\frac{n\pi}{L}\right)^2 - \tilde{k}^2}, \tag{3.2.17}$$

then

$$\tilde{\zeta}_0(x,y) = \sum_{n=0}^{\infty} a_n \cos\left(\frac{n\pi x}{L}\right) \cosh\left(\lambda_n y\right). \tag{3.2.18}$$

with coefficients a_n $(n > 0)$ such that

$$a_n = \frac{2}{L\lambda_n \sinh\left(\lambda_n D\right)} \int_0^L z(x) \cos\left(\frac{n\pi x}{L}\right) \mathrm{d}x \tag{3.2.19}$$

and

$$a_0 = \frac{1}{L\lambda_0 \sinh\left(\lambda_0 D\right)} \int_0^L z(x)\, \mathrm{d}x. \tag{3.2.20}$$

It is convenient to ignore the pathological case in which $\tilde{k}^2 = \left(\frac{n\pi}{L}\right)^2$ for some n, so their inequality will be assumed herewith.

Since the 0th order term in the asymptotic expansion for $\tilde{\zeta}$ has now been solved for, the 1st order term can be analysed. Gathering all relevant terms in (3.2.13) yields

$$\tilde{\zeta}_1 - \frac{\partial}{\partial x}\left(\frac{ghi}{\omega M_0}\frac{\partial\tilde{\zeta}_0}{\partial x} - \frac{gH_0 i}{\omega(\frac{rh}{H_0^2} + i\omega)}\frac{\partial\tilde{\zeta}_0}{\partial x} + \frac{gH_0 i}{\omega M_0}\frac{\partial\tilde{\zeta}_1}{\partial x}\right) - \frac{\partial}{\partial y}(...) = 0. \tag{3.2.21}$$

As with (3.2.14), this is a Helmholtz equation, albeit an inhomogeneous one:

$$\nabla^2\tilde{\zeta}_1 + \tilde{k}^2\tilde{\zeta}_1 = -A_{\tilde{\zeta}_0}(x,y). \tag{3.2.22}$$

The forcing function $A_{\tilde{\zeta}_0}$ depends only on $\tilde{\zeta}_0$, and is given by

$$A_{\tilde{\zeta}_0}(x,y) = \frac{\partial}{\partial x}\left[\left(\frac{h}{H_0} - \frac{M_0}{\frac{rh}{H_0^2} + i\omega}\right)\frac{\partial \tilde{\zeta}_0}{\partial x}\right] + \frac{\partial}{\partial y}\left[\left(\frac{h}{H_0} - \frac{M_0}{\frac{rh}{H_0^2} + i\omega}\right)\frac{\partial \tilde{\zeta}_0}{\partial y}\right]. \tag{3.2.23}$$

This forced Helmholtz equation with the inhomogeneous boundary at $y = D$ can be split up in two problems: one with inhomogeneous boundaries and homogeneous Helmholtz equation ($\tilde{\zeta}_1^a$) and one with homogeneous boundaries and inhomogeneous Helmholtz equation ($\tilde{\zeta}_1^b$). Because the procedure of solving for $\tilde{\zeta}_1^a$ is equivalent to the procedure to solve for $\tilde{\zeta}_0$, only the method to solve $\tilde{\zeta}_1^b$ will be discussed here. The related eigenvalue problem for $\tilde{\zeta}_1$ in terms of eigenfunctions ϕ is

$$(\nabla^2 + \tilde{k}^2)\phi = -\lambda\phi. \tag{3.2.24}$$

The standard solutions with the given Neumann boundaries are

$$\phi_{nm}(x,y) = \cos\left(\frac{n\pi x}{L}\right)\cos\left(\frac{m\pi y}{D}\right) \tag{3.2.25}$$

with eigenvalues $\lambda_{nm} = (\frac{n\pi}{L})^2 + (\frac{m\pi}{D})^2 - \tilde{k}^2$. Then, by eigenfunction expansion,

$$\tilde{\zeta}_1^b(x,y) = \sum_{n=0}^{\infty}\sum_{m=0}^{\infty} b_{nm}\phi_{nm}(x,y) \tag{3.2.26}$$

where the coefficients b_{nm} can be calculated as follows:

$$b_{nm} = \frac{4}{\lambda_{nm}LD}\iint_R A_{\tilde{\zeta}_0}(x,y)\phi_{nm}(x,y)\,d(x,y). \tag{3.2.27}$$

R is the concerned rectangular basin region. As with a previous paragraph, the assertion can be made that $b_{00} = 0$; to recap, this degree of freedom is created since only partial derivatives of $\tilde{\zeta}$ are prescribed on the boundaries of the systems that are concerned.

Second and higher orders of $\tilde{\zeta}_n = \tilde{\zeta}_n^a + \tilde{\zeta}_n^b$ can be calculated in a similar manner. By induction, each one of the equations will obey an inhomogeneous with similar inhomogeneous boundary conditions and inhomogeneous Helmholtz equations.

$$\nabla^2\tilde{\zeta}_n + \tilde{k}^2\tilde{\zeta}_n = -A_{\tilde{\zeta}_{n-1}}(x,y) \tag{3.2.28}$$

According to (3.2.13), each $A_{\tilde{\zeta}_p}$ contains $2p$ terms.

Having obtained $\tilde{\zeta}$ up to a desired degree by using this iterative process of solving for forced Helmholtz equations, the depth-averaged flows are calculated with equations (3.2.6) and (3.2.7):

$$\tilde{u} = -\frac{g}{M}\frac{\partial\tilde{\zeta}}{\partial x}, \quad \tilde{v} = -\frac{g}{M}\frac{\partial\tilde{\zeta}}{\partial y}.$$

3.3 Collocation Method

There are two suitable candidates to simulate the solutions for $\tilde{\zeta}$, $\tilde{u}$ and $\tilde{v}$. The main objective is to solve for the coefficients a_n and b_{nm}.
The first method has already been described by equations (3.2.19) and (3.2.27): this involves (numerical) integration to solve for an arbitrary amount of generalized Fourier coefficients.

As an alternative method, the collocation technique may be used, based on [1].
By differentiating $\tilde{\zeta}_0$ in the y-direction, the result is

$$\frac{\partial \tilde{\zeta}_0}{\partial y}(x,y) = \sum_{n=0}^{\infty} a_n \lambda_n \cos\left(\frac{n\pi x}{L}\right) \sinh(\lambda_n y). \tag{3.3.1}$$

The collocation method relies on selecting $N+1$ points $x_0, \ldots, x_N$ along the basin-sea interface, i.e. $y = D$, that avoid any boundary discontinuities, $x_0 \neq 0$, $x_N \neq L$. One then subsequently asserts that

$$\frac{\partial \tilde{\zeta}_0}{\partial y}(x_k,D) = \sum_{n=0}^{N} a_n \lambda_n \sinh(\lambda_n D) \cos\left(\frac{n\pi x_k}{L}\right) \tag{3.3.2}$$

holds for all $k = 0, \ldots, N$. See Figure 8.

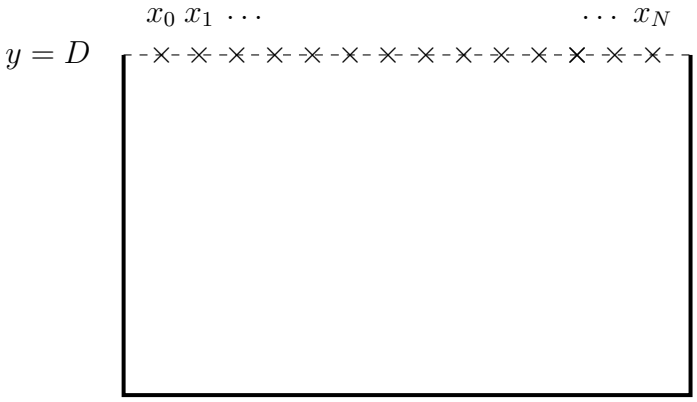

Figure 8: The collocation method.

Equation (3.3.2) defines a system of $N+1$ linear equations with the coefficients $a_0, \ldots, a_N$ as unknowns. Define

$$\phi_n(x) = \cos\left(\frac{n\pi x}{L}\right) \tag{3.3.3}$$

and

$$b_n = \lambda_n \sinh\left(\lambda_n D\right) \tag{3.3.4}$$

such that

$$z(x_k) = \frac{\partial \tilde{\zeta}_0}{\partial y}(x_k,D) = \sum_{n=0}^{\infty} a_n b_n \phi_n(x_k). \tag{3.3.5}$$

In matrix-vector notation, this can be written as

$$\begin{bmatrix} b_0\phi_0(x_0) & \dots & b_N\phi_N(x_0) \\ \vdots & \ddots & \vdots \\ b_0\phi_0(x_N) & \dots & b_N\phi_N(x_N) \end{bmatrix} \begin{bmatrix} a_0 \\ \vdots \\ a_N \end{bmatrix} = \begin{bmatrix} z(x_0) \\ \vdots \\ z(x_N) \end{bmatrix} \tag{3.3.6}$$

written as $B\mathbf{a} = \mathbf{z}$. The first $N+1$ coefficients can then be (uniquely) determined through $\mathbf{a} = B^{-1}\mathbf{z}$.
The collocation technique is a very convenient way to solve for coefficients, as will be shown in the next section, where the process of coupling multiple rectangular areas will be described in the context of a single inlet system.

3.4 Coupling of Multiple Basins

Now that the problem with a single rectangular basin has been discussed, it is time to extend the problem to the next stage. In this section, the influence of a rectangular inlet channel, attached to the earlier discussed rectangular basin, will be analysed. To address the problem of coupling rectangular modules together, a linear system of equations needs to be solved that determines the coefficients of the eigenfunction expanded solutions for $\tilde{\zeta}$ in adjacent basins. Suppose that a rectangular channel of width $\Delta L_1 = L_{1r} - L_{1l}$ with $L_{1r}, L_{1l} \in [0, L]$ and $L_{1r} > L_{1l}$, and length $\Delta D = D_1 - D$ with $D_1 > D$ is attached to the previously inspected rectangular basin, where the boundary $y = D_1$ forms the threshold between the ocean and the basin-inlet module couple. Note that the total system now is the one depicted in Figure 2. Define $\tilde{u}^{\mathrm{I}}$, $\tilde{v}^{\mathrm{I}}$ to be the time-independent flow velocities in the channel, and $\tilde{\zeta}^{\mathrm{I}}$ as the time-independent sea level disturbance in the channel.

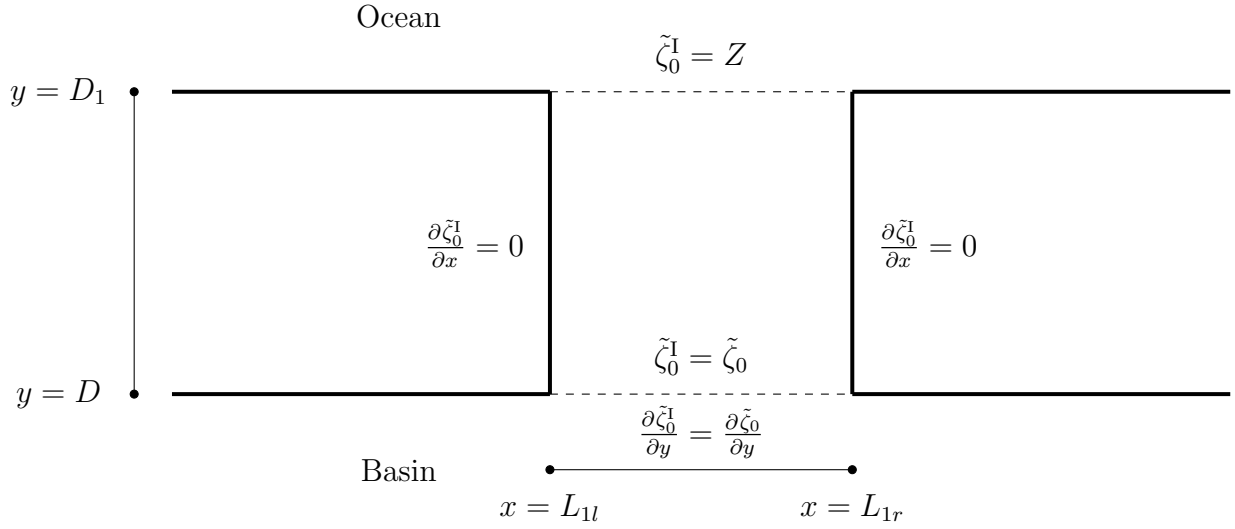

Figure 9: A rectangular channel that connects the basin to the ocean. The channel's coordinates and the boundary conditions for $\tilde{\zeta}_0^{\mathrm{I}}$ are indicated.

At this point, let $\tilde{\zeta}_0^{\mathrm{I}}(x,y)$ be the 0th order solution to equation (3.2.8) in the channel. Variations in bathymetry is a feature that will only be discussed in the main basin, so the water depth in the inlet channel, H^{I}, is considered to be constant. The solution of $\tilde{\zeta}_0^I$ satisfies the following boundary conditions [3]:

$$\begin{aligned} &\tilde{\zeta}_0^{\mathrm{I}}(x,D) = \tilde{\zeta}_0(x,D), \quad \frac{\partial \tilde{\zeta}_0^{\mathrm{I}}}{\partial y}(x,D) = \frac{\partial \tilde{\zeta}_0}{\partial y}(x,D), \\ &\frac{\partial \tilde{\zeta}_0^{\mathrm{I}}}{\partial x}(L_{1l},y) = 0 = \frac{\partial \tilde{\zeta}_0^{\mathrm{I}}}{\partial x}(L_{1r},y), \quad \tilde{\zeta}_0^{\mathrm{I}}(x,D_1) = Z. \end{aligned} \tag{3.4.1}$$

with some constant $Z > 0$. The last prescribed boundary condition simulates a single tidal consistuent of the ocean, which corresponds to a space-independent harmonic wave in the time-dependent problem:

$$\zeta_0^{\mathrm{I}}(x,D_1) = Ze^{-i\omega t}. \tag{3.4.2}$$

The equation that governs $\tilde{\zeta}_0^{\mathrm{I}}$ is related to a Helmholtz equation similar to (3.2.14) and can be directly derived by rewriting (3.2.8).

$$\tilde{\zeta}_0^{\mathrm{I}} - \frac{gH^{\mathrm{I}}i}{\omega M^{\mathrm{I}}}\left(\frac{\partial^2 \tilde{\zeta}_0^{\mathrm{I}}}{\partial x^2} + \frac{\partial^2 \tilde{\zeta}_0^{\mathrm{I}}}{\partial y^2}\right) = 0. \tag{3.4.3}$$

For convenience, define

$$(\tilde{k}^{\mathrm{I}})^2 = \frac{\omega M^{\mathrm{I}} i}{gH^{\mathrm{I}}} \tag{3.4.4}$$

and

$$\lambda_n^{\mathrm{I}} = \sqrt{\left(\frac{n\pi}{\Delta L_1}\right)^2 - (\tilde{k}^{\mathrm{I}})^2} \tag{3.4.5}$$

analogous to how $\tilde{k}^2$ and λ_n have been defined. The one-dimensional eigenfunctions for (3.4.3) can be determined through standard methods as usual,

$$X_n(x) = \cos\left(\frac{n\pi(x-L_{1l})}{\Delta L_1}\right), \quad Y_n(x) = \sinh\left(\lambda_n^{\mathrm{I}}(y-D_1)\right). \tag{3.4.6}$$

so that

$$\tilde{\zeta}_0^{\mathrm{I}}(x,y) = Z + \sum_{n=0}^{\infty} a_n^{\mathrm{I}} \cos\left(\frac{n\pi(x-L_{1l})}{\Delta L_1}\right) \sinh\left(\lambda_n^{\mathrm{I}}(y-D_1)\right). \tag{3.4.7}$$

The coefficients a_n^{I} are to be determined by relating them to a_n, the coefficients from the basin solution. For that purpose, one will consider the boundary conditions that $\tilde{\zeta}_0(x,D) =$

[3] Formally, $\frac{\partial \tilde{\zeta}_0^{\mathrm{I}}}{\partial y}(x,D) = \frac{\partial \tilde{\zeta}_0}{\partial y}(x,D)$ does not necessarily hold, but $H^{\mathrm{I}}u^{\mathrm{I}}(x,D) = H(x,D)u(x,D)$, due to conservation of momentum. However, one will assume that $H(x,D) = H^{\mathrm{I}}$; this results in both conditions becoming equivalent.

$\tilde{\zeta}_0^{\mathrm{I}}(x,D)$ and $\frac{\partial\tilde{\zeta}_0}{\partial y}(x,D) = \frac{\partial\tilde{\zeta}_0^{\mathrm{I}}}{\partial y}(x,D)$ for every x on the channel-basin boundary:

$$\begin{aligned}\tilde{\zeta}_0(x,D) &= \sum_{n=0}^{\infty} a_n \cos\left(\frac{n\pi x}{L}\right)\cosh\left(\lambda_n D\right)\\ = Z + \sum_{n=0}^{\infty} a_n^{\mathrm{I}} \cos\left(\frac{n\pi(x-L_{1l})}{\Delta L_1}\right)&\sinh\left(\lambda_n^{\mathrm{I}}(D-D_1)\right) = \tilde{\zeta}_0^{\mathrm{I}}(x,D)\end{aligned} \tag{3.4.8}$$

and

$$\begin{aligned}\frac{\partial\tilde{\zeta}_0}{\partial y}(x,D) &= \sum_{n=0}^{\infty} a_n\lambda_n \sinh\left(\lambda_n D\right)\cos\left(\frac{n\pi x}{L}\right)\\ = \sum_{n=0}^{\infty} a_n^{\mathrm{I}}\lambda_n^{\mathrm{I}} \cosh\left(\lambda_n^{\mathrm{I}}(D-D_1)\right)&\cos\left(\frac{n\pi(x-L_{1l})}{\Delta L_1}\right) = \frac{\partial\tilde{\zeta}_0^{\mathrm{I}}}{\partial y}(x,D).\end{aligned} \tag{3.4.9}$$

In addition, a no-flow boundary condition holds for every x on the line $y = D$ that is not situated on the basin-inlet boundary.

$$\frac{\partial\tilde{\zeta}_0}{\partial y}(x,D) = \sum_{n=0}^{N} a_n\lambda_n \sinh(\lambda_n D)\cos\left(\frac{n\pi x}{L}\right) = 0 \tag{3.4.10}$$

As before, by truncating the infinite series for the sea level perturbation, a linear system is found from which a finite number of coefficients are solved. Suppose there are $N+1$ points to be taken from the concerned region along the line $y = D$, labeled $x_0, \ldots, x_N$, of which $M+1$ points coincide with the channel border. For convenience's sake, let the ith through the jth points be these described points ($0 \le i \le j \le N$, $M = j - i$). See Figure 10.

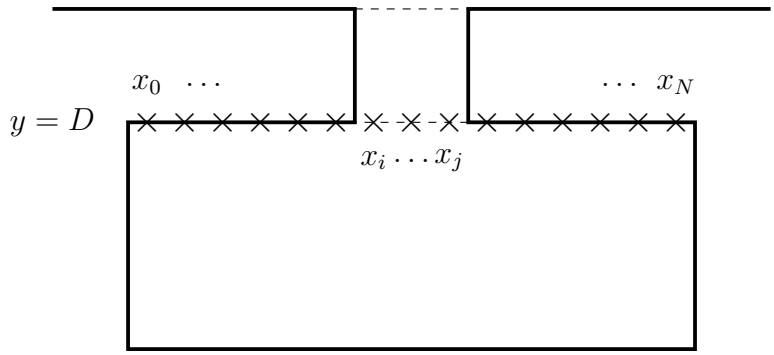

Figure 10: The collocation method applied to the basin-inlet boundary.

In addition, let

$$\begin{aligned} b_n &:= \cosh\left(\lambda_n D\right)\\ b_n^{\mathrm{I}} &:= \sinh\left(\lambda_n^{\mathrm{I}}(D-D_1)\right)\\ b_n' &:= \lambda_n \sinh\left(\lambda_n D\right)\\ b_n^{\mathrm{I}'} &:= \lambda_n^{\mathrm{I}} \cosh\left(\lambda_n^{\mathrm{I}}(D-D_1)\right)\end{aligned} \tag{3.4.11}$$

and

$$\phi_n(x) := \cos\left(\frac{n\pi x}{L}\right), \quad \phi_n^{\mathrm{I}}(x) := \cos\left(\frac{n\pi(x - L_{1l})}{\Delta L_1}\right). \tag{3.4.12}$$

The expressions in (3.4.11) and (3.4.12) can now be used to rewrite the truncated series based on the series for $\tilde{\zeta}_0$ and $\tilde{\zeta}_0^{\mathrm{I}}$ in (3.4.8), (3.4.9) and (3.4.10). By collocation, one asserts that, for all $p = i, \ldots, j$ and $k = 0, \ldots i-1, j+1, \ldots, N$,

$$\begin{aligned} \sum_{n=0}^{N} a_n b_n \phi_n(x_k) &= 0 \\ \sum_{n=0}^{N} a_n b_n \phi_n(x_p) - \sum_{m=0}^{M} a_m^{\mathrm{I}} b_m^{\mathrm{I}} \phi_m^{\mathrm{I}}(x_p) &= Z \\ \sum_{n=0}^{N} a_n b_n' \phi_n(x_p) - \sum_{m=0}^{M} a_m^{\mathrm{I}} b_m^{\mathrm{I}'} \phi_m^{\mathrm{I}}(x_p) &= 0 \end{aligned} \tag{3.4.13}$$

With the given definitions and assertions, the following $N + M + 2$ matrix equation can be derived.

$$\begin{bmatrix} b_0'\phi_0(x_0) & \ldots & b_N'\phi_N(x_0) & 0 & \ldots & 0 \\ \vdots & \ddots & \vdots & \vdots & \ddots & \vdots \\ b_0'\phi_0(x_i) & \ldots & b_N'\phi_N(x_i) & -b_0^{\mathrm{I}'}\phi_0^{\mathrm{I}}(x_i) & \ldots & -b_M^{\mathrm{I}'}\phi_M^{\mathrm{I}}(x_i) \\ \vdots & \ddots & \vdots & \vdots & \ddots & \vdots \\ b_0'\phi_0(x_j) & \ldots & b_N'\phi_N(x_j) & -b_0^{\mathrm{I}'}\phi_0^{\mathrm{I}}(x_j) & \ldots & -b_M^{\mathrm{I}'}\phi_M^{\mathrm{I}}(x_j) \\ \vdots & \ddots & \vdots & \vdots & \ddots & \vdots \\ b_0'\phi_0(x_N) & \ldots & b_N'\phi_N(x_N) & 0 & \ldots & 0 \\ b_0\phi_0(x_i) & \ldots & b_N\phi_N(x_i) & -b_0^{\mathrm{I}}\phi_0^{\mathrm{I}}(x_i) & \ldots & -b_M^{\mathrm{I}}\phi_M^{\mathrm{I}}(x_i) \\ \vdots & \ddots & \vdots & \vdots & \ddots & \vdots \\ b_0\phi_0(x_j) & \ldots & b_N\phi_N(x_j) & -b_0^{\mathrm{I}}\phi_0^{\mathrm{I}}(x_j) & \ldots & -b_M^{\mathrm{I}}\phi_M^{\mathrm{I}}(x_j) \end{bmatrix} \begin{bmatrix} a_0 \\ \vdots \\ a_N \\ a_0^{\mathrm{I}} \\ \vdots \\ a_M^{\mathrm{I}} \end{bmatrix} = \begin{bmatrix} 0 \\ \vdots \\ 0 \\ \vdots \\ 0 \\ \vdots \\ 0 \\ Z \\ \vdots \\ Z \end{bmatrix} \tag{3.4.14}$$

Compare the expressions in (3.4.13) and (3.4.14) with the earlier results in (3.3.5) and (3.3.6). The solution to the first $N+1$ coefficients in the basin as well as the first $M+1$ coefficients in the channel can be determined by inverting the equation.

3.5 Computational Approach

The coefficients as defined in (3.4.11) are generally not efficient to use in a matrix in order to solve for the modal coefficients, since D is usually quite large (tens of kilometers). This in turn will lead to extremely large matrix coefficients, which results in a matrix that is singular from a computational point of view. This can be remedied by choosing the composing eigenfunctions more carefully, so that the coefficients from (3.4.11) can be replaced by similar numbers that are bounded in magnitude.

Instead of opting for the hyperbolic cosine in (3.2.18), two exponentials may be used to

express it. Note that

$$a_n \cosh(\lambda_n y) = \frac{a_n}{2}\left(e^{\lambda_n y} + e^{-\lambda_n y}\right) = a_{1n}e^{\lambda_n(y-D)} + a_{2n}e^{-\lambda_n y}, \tag{3.5.1}$$

where

$$a_{1n} = \frac{a_n}{2}e^{\lambda_n D}, \quad a_{2n} = \frac{a_n}{2}. \tag{3.5.2}$$

Similar alternations can be made regarding $\frac{\partial\tilde{\zeta}_0}{\partial y}$, $\tilde{\zeta}_0^{\mathrm{I}}$ and $\frac{\partial\tilde{\zeta}_0^{\mathrm{I}}}{\partial y}$. At the basin-channel boundary $x = D$, one will have:

$$\begin{aligned}\tilde{\zeta}_0(x,D) &= \sum_{n=0}^{\infty}\left(a_{1n} + a_{2n}e^{-\lambda_n D}\right)\cos\left(\frac{n\pi x}{L}\right)\\ &= Z + \sum_{n=0}^{\infty}\left(a_{1n}^{\mathrm{I}}e^{\lambda_n^{\mathrm{I}}(D-D_1)} - a_{2n}^{\mathrm{I}}\right)\cos\left(\frac{n\pi(x-L_{1l})}{\Delta L_1}\right) = \tilde{\zeta}_0^{\mathrm{I}}(x,D),\end{aligned} \tag{3.5.3}$$

$$\begin{aligned}\frac{\partial\tilde{\zeta}_0}{\partial y}(x,D) &= \sum_{n=0}^{\infty}\lambda_n\left(a_{1n} - a_{2n}e^{-\lambda_n D}\right)\cos\left(\frac{n\pi x}{L}\right)\\ &= \sum_{n=0}^{\infty}\lambda_n^{\mathrm{I}}\left(a_{1n}^{\mathrm{I}}e^{\lambda_n^{\mathrm{I}}(D-D_1)} + a_{2n}^{\mathrm{I}}\right)\cos\left(\frac{n\pi(x-L_{1l})}{\Delta L_1}\right) = \frac{\partial\tilde{\zeta}_0^{\mathrm{I}}}{\partial y}(x,D).\end{aligned} \tag{3.5.4}$$

The amount of Fourier coefficients one has to solve for has now seemingly doubled, but some rewriting will demonstrate that this number of unknowns remains the same. Remember the assertion that

$$\frac{\partial\tilde{\zeta}_0}{\partial y}(x,0) = \sum_{n=0}^{\infty}\lambda_n\left(a_{1n}e^{-\lambda_n D} - a_{2n}\right)\cos\left(\frac{n\pi x}{L}\right) = 0 \tag{3.5.5}$$

so

$$a_{1n}e^{-\lambda_n D} = a_{2n} \tag{3.5.6}$$

which exactly aligns with equation (3.5.2). Also,

$$\begin{aligned}\tilde{\zeta}_0^{\mathrm{I}}(x,D_1) = Z + \sum_{n=0}^{\infty}\left(a_{1n}^{\mathrm{I}} - a_{2n}^{\mathrm{I}}e^{-\lambda_n^{\mathrm{I}}(D_1-D)}\right)\cos\left(\frac{n\pi(x-L_{1l})}{\Delta L_1}\right)\\ = Z.\end{aligned} \tag{3.5.7}$$

meaning that

$$a_{1n}^{\mathrm{I}} = a_{2n}^{\mathrm{I}}e^{-\lambda_n^{I}(D_1-D)}. \tag{3.5.8}$$

Taking all this together, it is found that

$$\tilde{\zeta}_0(x,y) = \sum_{n=0}^{\infty}\left(a_{1n}e^{\lambda_n(y-D)} + a_{2n}e^{-\lambda_n y}\right)\cos\left(\frac{n\pi x}{L}\right) \tag{3.5.9}$$

$$\tilde{\zeta}_0^{\mathrm{I}}(x,y) = Z + \sum_{n=0}^{\infty}\left(a_{1n}^{\mathrm{I}}e^{\lambda_n^{\mathrm{I}}(y-D_1)} - a_{2n}^{\mathrm{I}}e^{-\lambda_n^{\mathrm{I}}(y-D)}\right)\cos\left(\frac{n\pi(x-L_{1l})}{\Delta L_1}\right). \tag{3.5.10}$$

Using conditions (3.5.6) and (3.5.8) for the coefficients, $\tilde{\zeta}_0$ and $\tilde{\zeta}_0^{\mathrm{I}}$ can be rewritten.

$$\tilde{\zeta}_0(x,y) = \sum_{n=0}^{\infty} a_n \left(e^{\lambda_n(y-D)} + e^{-\lambda_n(y+D)}\right) \cos\left(\frac{n\pi x}{L}\right), \tag{3.5.11}$$

$$\tilde{\zeta}_0^{\mathrm{I}}(x,y) = Z + \sum_{n=0}^{\infty} a_n^{\mathrm{I}} \left(e^{\lambda_n^{\mathrm{I}}(y-2D_1+D)} - e^{-\lambda_n^{\mathrm{I}}(y-D)}\right) \cos\left(\frac{n\pi(x-L_{1l})}{\Delta L_1}\right). \tag{3.5.12}$$

These alternate expressions for $\tilde{\zeta}_0$ and $\tilde{\zeta}_0^{\mathrm{I}}$ now contain coefficient parts that remain bounded. To construct a collocation matrix equation, the boundaries are examined:

$$\tilde{\zeta}_0(x,D) = \sum_{n=0}^{\infty} a_n \left(1 + e^{-2\lambda_n D}\right) \cos\left(\frac{n\pi x}{L}\right) \tag{3.5.13}$$

$$\tilde{\zeta}_0^{\mathrm{I}}(x,D) = Z + \sum_{n=0}^{\infty} a_n^{\mathrm{I}} \left(e^{2\lambda_n^{\mathrm{I}}(D-D_1)} - 1\right) \cos\left(\frac{n\pi(x-L_{1l})}{\Delta L_1}\right) \tag{3.5.14}$$

$$\frac{\partial\tilde{\zeta}_0}{\partial y}(x,D) = \sum_{n=0}^{\infty} a_n\lambda_n \left(1 - e^{-2\lambda_n D}\right) \cos\left(\frac{n\pi x}{L}\right) \tag{3.5.15}$$

$$\frac{\partial\tilde{\zeta}_0^{\mathrm{I}}}{\partial y}(x,D) = \sum_{n=0}^{\infty} a_n^{\mathrm{I}}\lambda_n^{\mathrm{I}} \left(e^{2\lambda_n^{\mathrm{I}}(D-D_1)} + 1\right) \cos\left(\frac{n\pi(x-L_{1l})}{\Delta L_1}\right) \tag{3.5.16}$$

Define, analogous to (3.4.11),

$$\begin{aligned} \beta_n &:= 1 + e^{-2\lambda_n D} \\ \beta_n^{\mathrm{I}} &:= e^{2\lambda_n^{\mathrm{I}}(D-D_1)} - 1 \\ \beta_n' &:= \lambda_n \left(1 - e^{-2\lambda_n D}\right) \\ \beta_n^{\mathrm{I}'} &:= \lambda_n^{\mathrm{I}} \left(e^{2\lambda_n^{\mathrm{I}}(D-D_1)} + 1\right) \end{aligned} \tag{3.5.17}$$

This creates a matrix equation similar to the one in (3.4.14), however computationally much more tractable.

3.6 First and Higher Order Channel Solutions

Now that the 0th order solution $\tilde{\zeta}_0^{\mathrm{I}}$ has been accounted for, it is time to solve for the first order solution in the inlet channel. If one assumes that the ocean is sufficiently unaffected by any changes in the basin-channel system, the only first order perturbation that the channel will receive originates from the basin. In the channel, one therefore has

- One homogeneous Dirichlet boundary at $y = D_1$.
- Two homogeneous Neumann boundary at $x = L_{1l}$ and $x = L_{1r}$.
- One prescribed Dirichlet boundary at $x = D$, namely $\frac{\partial\tilde{\zeta}_1^{\mathrm{I}}}{\partial y}(x,D) = \frac{\partial\tilde{\zeta}_1}{\partial y}(x,D)$

- One prescribed Neumann boundary at $x = D$, namely $\tilde{\zeta}_1^{\mathrm{I}}(x, D) = \tilde{\zeta}_1(x, D)$

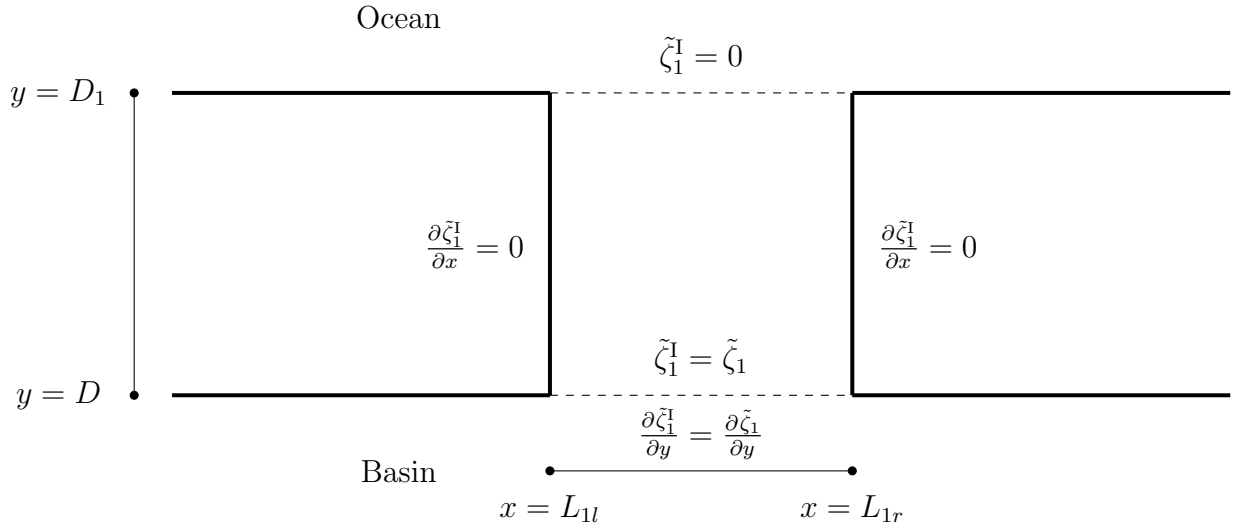

Figure 11: The inlet channel with coordinates and boundary conditions for $\tilde{\zeta}_1^{\mathrm{I}}$.

$\tilde{\zeta}_1^{\mathrm{I}}$ obeys the equation (3.4.3) in the channel, thus one can write down the general solution as usual.

$$\tilde{\zeta}_1^{\mathrm{I}}(x, y) = \sum_{n=0}^{\infty} a_{1,n}^{\mathrm{I}} \cos\left(\frac{n\pi(x - L_{1l})}{\Delta L_1}\right)\left(e^{\lambda_n^{\mathrm{I}}(y-2D_1+D)} - e^{-\lambda_n^{\mathrm{I}}(y-D)}\right). \tag{3.6.1}$$

To find these coefficients, the standard method of integration can be used.

$$a_{1,n}^{\mathrm{I}} = \frac{2}{\Delta L_1 \beta_n^{\mathrm{I}\prime}} \int_{L_{1l}}^{L_{1r}} \frac{\partial \tilde{\zeta}_1}{\partial y}(x, D) \cos\left(\frac{n\pi(x - L_{1l})}{\Delta L_1}\right) \mathrm{d}x. \tag{3.6.2}$$

It should be noted that a collocation technique is not directly a viable choice to solve for $a_{1,n}^{\mathrm{I}}$, as these involve only one degree of separation, whereas the coefficients b_{nm} associated with $\tilde{\zeta}_1$ involve two. Because of the discrepancy between how the modes that construct $\tilde{\zeta}_1^{\mathrm{I}}$ and $\tilde{\zeta}_1$ are numbered, the collocation method as described in section 3.4 can not be readily used to solve for a finite amount of coefficients.
Having solved for a sufficient amount of $a_{1,n}^{\mathrm{I}}$ through (3.6.2), the x and y-directional partial derivatives of $\tilde{\zeta}_1^{\mathrm{I}}$ can be calculated by simply differentiating the structural parts of the expression as indicated in (3.6.1). This needs to be done in order to calculate the flow velocities in the channel, by using (3.2.6) and (3.2.7) as per usual:

$$\tilde{u}^{\mathrm{I}} = -\frac{g}{M}\frac{\partial \tilde{\zeta}^{\mathrm{I}}}{\partial x},$$
$$\tilde{v}^{\mathrm{I}} = -\frac{g}{M}\frac{\partial \tilde{\zeta}^{\mathrm{I}}}{\partial y}.$$

Generally speaking, for every order of $\tilde{\zeta}_m$ one solves in the basin, one is able to solve the corresponding order of $\tilde{\zeta}_m^{\mathrm{I}}$ in the channel, in a form similar to (3.6.1);

$$\tilde{\zeta}_m^{\mathrm{I}}(x,y) = \sum_{n=0}^{\infty} a_{m,n}^{\mathrm{I}} \cos\left(\frac{n\pi(x-L_{1l})}{\Delta L_1}\right)\left(e^{\lambda_n^{\mathrm{I}}(y-2D_1+D)} - e^{-\lambda_n^{\mathrm{I}}(y-D)}\right), \tag{3.6.3}$$

where

$$a_{m,n}^{\mathrm{I}} = \frac{2}{\Delta L_1 \beta_n^{\mathrm{I}\prime}} \int_{L_{1l}}^{L_{1r}} \frac{\partial \tilde{\zeta}_m}{\partial y}(x,D) \cos\left(\frac{n\pi(x-L_{1l})}{\Delta L_1}\right) \mathrm{d}x. \tag{3.6.4}$$

With all of the analysed matter taken into consideration, one has fully solved the shallow water equations in a single-inlet system, given specific types of basin bathymetry that exhibit small variations.

4 Results

In this chapter, some applications of the theory described in the previous section will be shown. All simulations are implemented and performed in MATLAB version 2015b [6], and the numerical values that have been used are found in the Appendix.

4.1 Integration-Collocation comparison

The first result that will be shown is the effectiveness of calculating modal coefficients by means of the collocation technique. This will be compared with another conventional method, which is the method of obtaining coefficients through integration, explained in section 3.3. The geometry for which this comparison will be shown is the basin that is directly coupled to the ocean, as shown in section 3.3. Here, 50 modes will be used to reconstruct $\tilde{\zeta}_0$. However, unlike the initially proposed collocation method in section 3.4, the computational variant as described in section 3.6 will be adopted to provide the simulation. For this purpose, matrix equation (3.3.6) remains unchanged, but the accompanying matrix coefficients are defined as

$$b_n = \lambda_n(1 - e^{-2\lambda_n D}), \tag{4.1.1}$$

in accordance with the coefficients defined in (3.5.17).

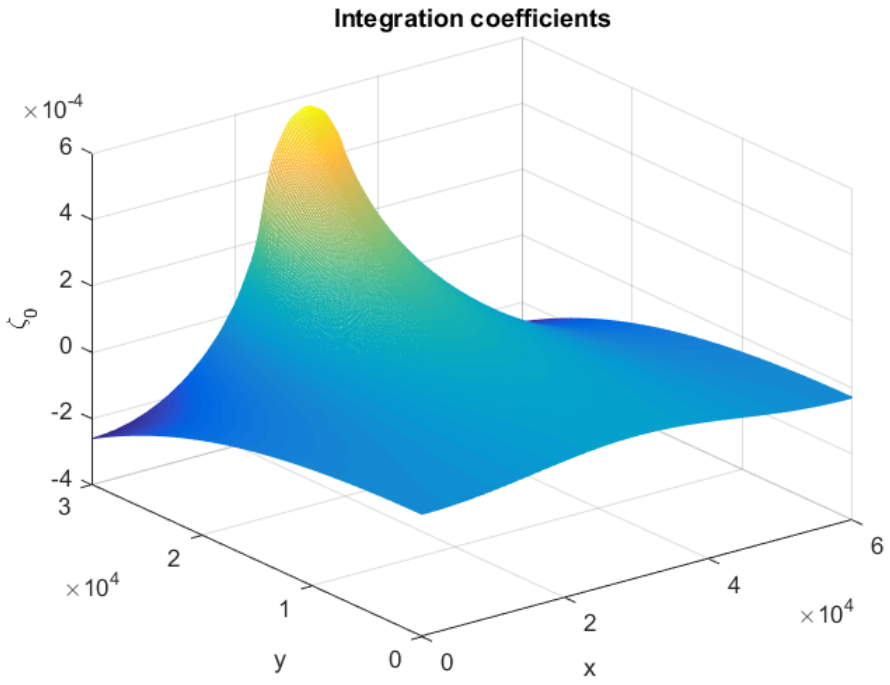

Figure 12: Integration method applied to solve 50 modes of the 0th order basin solution.

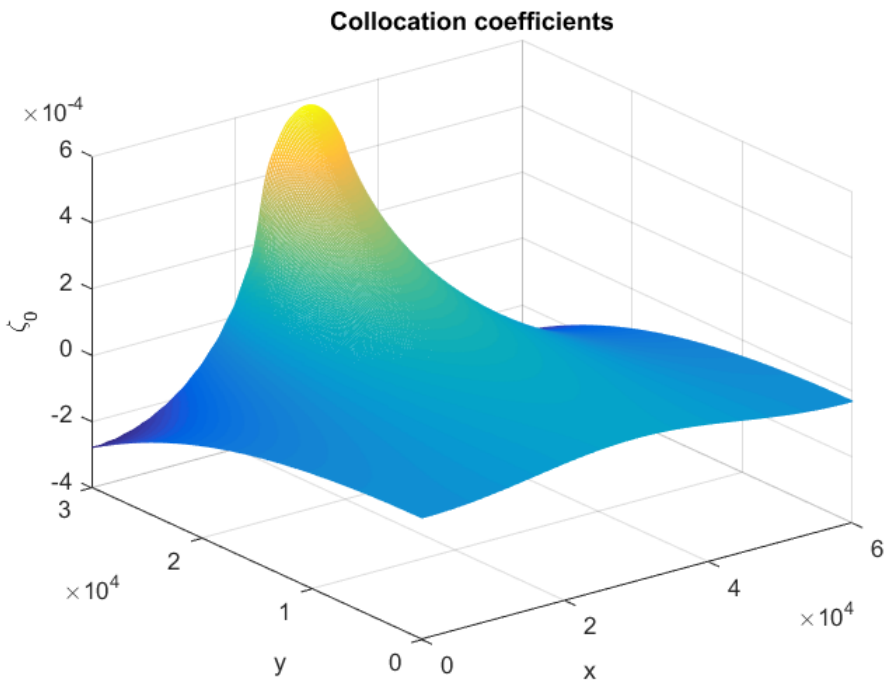

Figure 13: Collocation method applied to solve the same problem.

From the lack of distinction between these figures, it can be concluded that both methods work approximately equally well as to solve for the coefficients. The average difference between both methods is $4.909 \cdot 10^{-6}$, which is about 6% of of the average magnitude of $\tilde{\zeta}_0$.

4.2 Basin Water Depths and Flow Simulations

The core of this project is to analyse how variations in basin water depth $H(x, y)$ lead to differences in flow velocities through inlet channels. Therefore, it is necessary to consider different types of $h(x, y)$ and discuss their effects accordingly.
Three bathymetries will be discussed here.

- A flat seabed;
- Accumulation of sediment near the line $x = 0$ and $x = L$;
- Accumulation of sediment further away from the basin-inlet interface.

These shapes are respectively defined as:

$$h(x, y) = 0; \quad \frac{H_0}{(x - \frac{L}{2})^2 + (y - D)^2}; \quad H_0 \cos^2\left(\frac{3x}{L}\right), \tag{4.2.1}$$

and can be viewed in Figure 14.

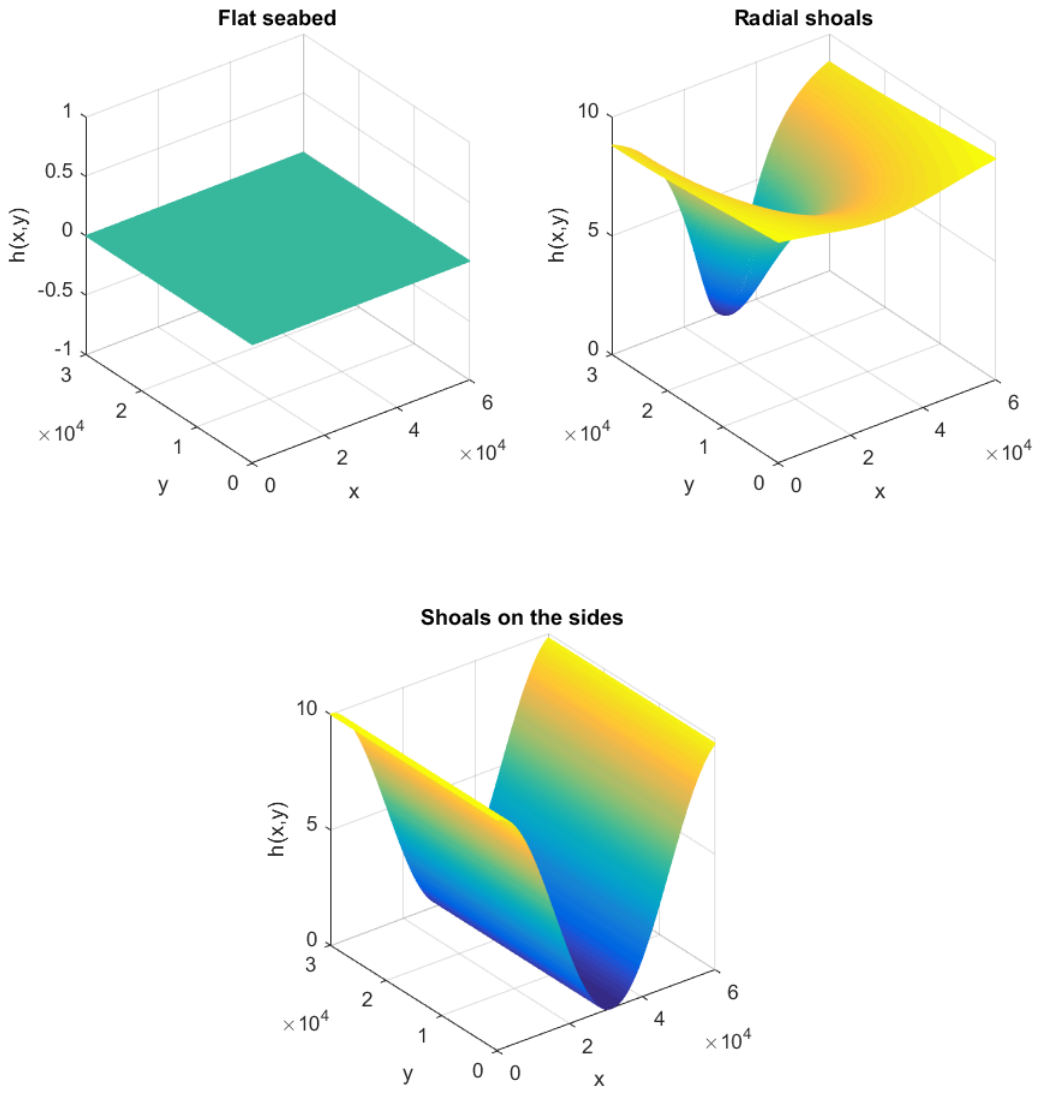

Figure 14: Various possible basin depth variations.

Taking $\delta = 1$ and noting that H_0 and $h(x, y)$ are both in the order of 10 m, one can see that $\delta \frac{h}{H_0} < 1$, which makes the geometric expansions in e.g. (3.2.10) valid. These bottom variations lead to the following first order flow velocity patterns in the inlet channel (Figure 15). During this calculation, a central difference method is applied to solve for the Helmholtz forcing term $A_{\tilde{\zeta}_0}$, (3.2.23).

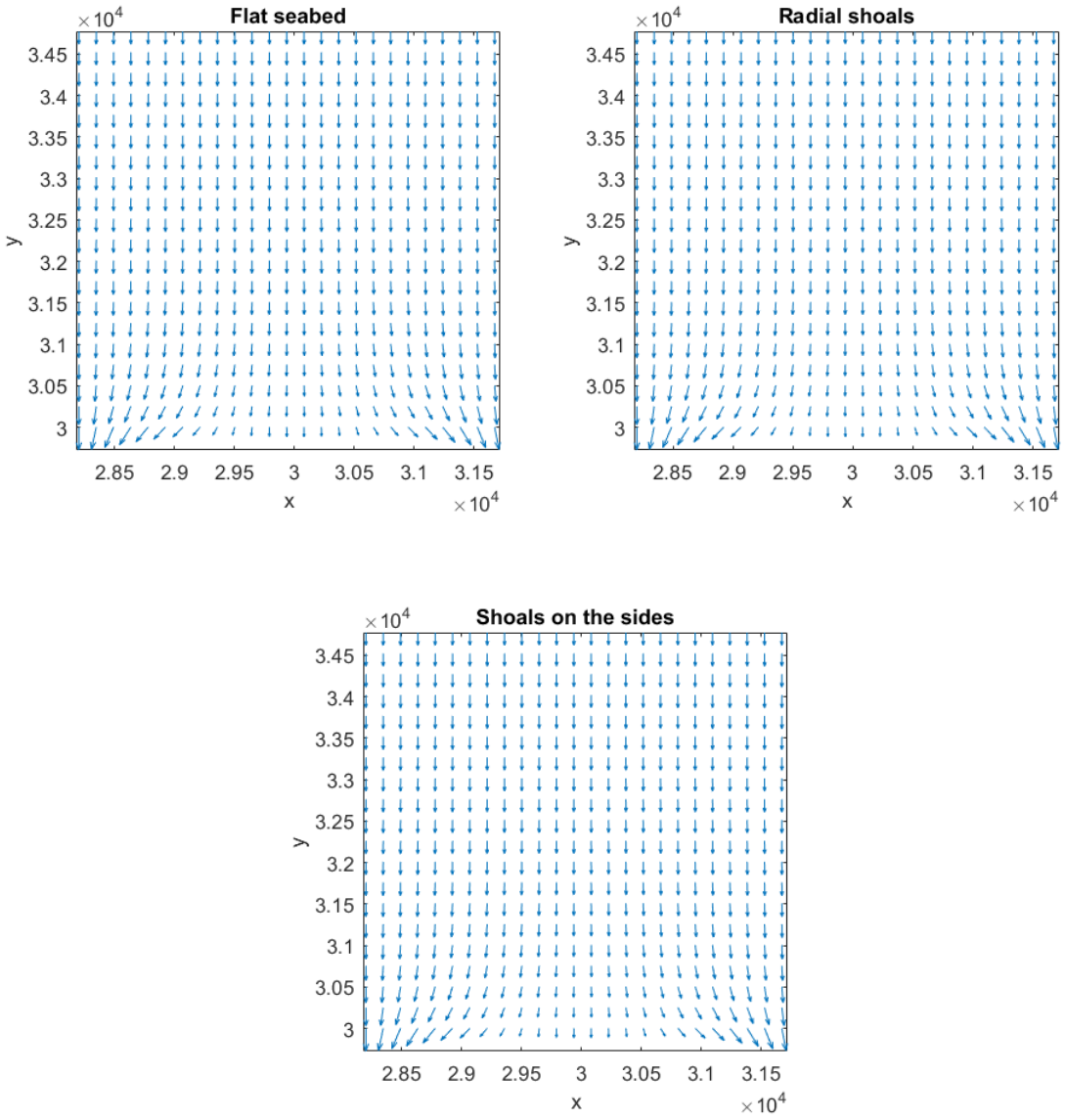

Figure 15: Velocity vector fields in the inlet channel due to the type of forcing indicated in the titles.

From this figure, it is not immediately obvious that different basin bathymetries influence water flow patterns in the adjacent inlet channel. This is due to the fact that the pertubations in the bathymetries are limited in size compared to the constant order term. However, on careful inspection, the flow velocities do differ from each other. The velocities U are numerically calculated to be 0.13645, 0.13652 and 0.13649 respectively (in m s^{-1}). These results indicate that all three inlet channels will have a decreasing cross-sectional area as time progresses. It also shows that the system with radial shoals are the most stable, since this number is the closest to $U_{eq} = 1$ m s^{-1}.

5 Discussion and Conclusion

In this thesis, a prediction has been made concerning how the cross-sectional area of the tidal channel behaves over time. For this purpose, the shallow water equations have been introduced and analysed, and some results have been deduced from Escoffier's principle.
A number of simplifications have been made to carry out the analyses of the shallow water equations. However, by taking some factors into account that have been ignored, this model - along with Escoffier's principle - might lead to more accurate predictions of the cross-sectional size of inlets.
First of all, the friction coefficient is assumed to be constant throughout the single-inlet system, while this of course is not the case in a physically accurate system. As bottom friction generally is related to the water flow velocities, these coefficients are to be calculated by means of an iterative process, see e.g. [1].
The Coriolis parameter f has been assumed to be negligible throughout most of the research. Though this is physically accurate for any system located on the equator ($\theta = 0$), this assumption becomes increasingly invalid further away from the equator. For instance, the Waddeneilanden barrier islands are located at approximately $\theta = 54°$, which means that $f = 1.18 \cdot 10^{-4}$ rad s^{-1}. In that case, f is in the same order of the friction coefficient r. However, allowing f to take on non-zero values leads to boundary conditions that are not easily analysed, as mentioned in section 3.1, (3.1.13), and fall outside the scope of this thesis.
Another consideration that falls outside of the scope of this thesis is the analysis of multiple inlet systems, see for instance [1] for the double inlet system or [2] for the analysis of a system with many inlets. In principle, any number of inlet channels may be used to attach the basin to the ocean, and be solved and simulated in a very similar manner as described in sections 3.4 and 3.6.
This research was mainly devoted to obtain analytical expressions of sea level perturbations and flow velocities. The method hinges on perturbation theory, which demands that the variations in basin bathymetry $\delta h(x, y)$ is small with respect to its constant term H_0. However, as one might suggest, this is not the case for any general basin bathymetry $H(x, y)$. In that case, a numerical approach of the linearised shallow water equations become practically inevitable. For a closer research on numerical schemes involving this equation system, further knowledge in advanced numerical methods is required. Some results can be found in [5]. Other similar aspects that have not been accounted for during this thesis is the discussion on which numerical methods are used to fully integrate Escoffier's equation (2.2.1), as well as any numerical truncation and rounding errors when applying the numerical partial derivative scheme.

Taking this all together, it can be concluded that this thesis has resulted in an analytical solution to the shallow water equations. The solution is subsequentially used to predict any changes in the cross-sectional area of the inlet channel in the single-inlet system. This thesis forms a solid basis for future researches on inlet system stability, especially those involving the numerical aspects.

Appendix A: Numerical values

To address the problems that are discussed in this thesis, a number of relevant physical quantities concerning the basin-inlet-ocean problem are introduced in order to establish relationships between one another. As reference for these quantities, their numerical values and their concise definitions, this lookup table is composed. These are largely based on the values used in [1].

D :	y-dimension of basin	$20 \cdot 10^3$ m
f :	Coriolis parameter	0 rad s^{-1}
g :	Gravitational acceleration	9.81 m s^{-2}
H_0 :	0th order basin water depth	10 m
H^{I} :	Inlet channel water depth	10 m
L :	x-dimension of basin	$200 \cdot 10^3$ m
r :	Seafloor friction coefficient	10^{-4}
U_{eq} :	Equilibrium speed of inlet flow	1 m s^{-1}
δ :	Small parameter	0.1
ΔD :	y-dimension of inlet channel	$5 \cdot 10^3$ m
ΔL_1 :	x-dimension of inlet channel	$3.6 \cdot 10^3$ m
κ :	Transport power law coefficient	3
μ :	Sediment import	$1.6 \cdot 10^{-2}$ m^3 s^{-1}
ω :	Tidal frequency	$1.4 \cdot 10^{-4}$ rad s^{-1}

Appendix B: MATLAB source code

The MATLAB code for generating the plots in Chapter 4 (Results), as well as any numerical calculations that have been mentioned, can be found below.

```
clear; clc; close all;
format longG; format compact;

%% 0 order zeta

L = 60E3; D = 30E3;
Nmeshx = 250; Nmeshy = 200;
x = linspace(0,L,Nmeshx);
y = linspace(0,D,Nmeshy);
[X,Y] = meshgrid(x,y);

H0 = 5;
omega = 1.4E-4;
g = 9.81;
r = 1E-4;
M0 = r/H0 - 1i*omega;
K = omega*M0*1i./(g*H0);

z = @(x) 1E-7.*(heaviside(x - 0.4.*L) - heaviside(x - 0.6.*L));
lambda = @(n) sqrt((n*pi/L)^2 - K);

Phi = @(n) cos(n.*pi.*X./L).*(exp(lambda(n).*(Y - D)) + exp(-lambda(n).*(Y
    + D)));
Phix = @(n) -n.*pi./L.*sin(n.*pi.*X./L).*(exp(lambda(n).*(Y - D)) + exp(-
   lambda(n).*(Y + D)));
Phiy = @(n) lambda(n).*cos(n.*pi.*X./L).*(exp(lambda(n).*(Y - D)) - exp(-
   lambda(n).*(Y + D)));

% Number of 0th order modes
N = 50;

x1 = L/(N + 1).*(0.5 + 0:(N + 1))';

psi = @(n) cos(n.*pi.*x1./L);
bd = @(n) lambda(n).*(1 - exp(-2.*lambda(n).*D));

%% Coefficients by collocation
B = zeros(N + 1);
for i = 0:N
    B(:,i + 1) = bd(i).*psi(i);
end
Z = z(x1);
A = B\Z;

Zeta0m = zeros(Nmeshx,Nmeshy)';
for i = 2:N + 1
    Zeta0m = Zeta0m + A(i).*Phi(i - 1);
end
```

```
figure;
mesh(X,Y,real(Zeta0m));
xlabel x
ylabel y
zlabel \zeta_0; title('Collocation␣coefficients')

%% Coefficients by integrating
a = @(n) (n ~= 0).*2./(L.*lambda(n).*(1 - exp(-2.*lambda(n).*D)))*trapz(x,
   z(x).*cos(n.*pi.*x./L));

Zeta0 = zeros(Nmeshx,Nmeshy)';
Zeta0x = zeros(Nmeshx,Nmeshy)';
Zeta0y = zeros(Nmeshx,Nmeshy)';
for i = 0:N - 1
    Zeta0 = Zeta0 + a(i).*Phi(i);
    Zeta0x = Zeta0x + a(i).*Phix(i);
    Zeta0y = Zeta0y + a(i).*Phiy(i);
end

figure; mesh(X,Y,real(Zeta0)); xlabel x; ylabel y; zlabel \zeta_{0};
title('Integration␣coefficients')

% Average difference between both methods
avgdiff = mean2(abs(Zeta0m - Zeta0));
```

```
clear; clc; close all;
format longG; format compact;

%% Parameters and geometries

% Basin dimensions
L = 60E3; D = 30E3; H0 = 10;

% Inlet channel dimensions
D1 = 35E3; L1l = 0.47*L; L1r = 0.53*L; deltaL1 = L1r - L1l;
HI = 10;

% Prescribed sea level perturbation at inlet-ocean interface
Z = 0.1;

% Global quantities
omega = 1.4E-4; % Tidal frequency
g = 9.81; % Gravitational acceleration
r = 1E-4; % Bottom friction coefficient

M0 = r/H0 - 1i*omega; MI = r/HI - 1i*omega; % M-term
K = omega*M0*1i./(g*H0); K1 = omega*MI*1i./(g*HI); % Wave number

% Number of mesh points (basin and inlet channel)
Nmeshx = 250; Nmeshy = 200;

% Basin
x = linspace(0,L,Nmeshx);
```

```
y = linspace(0,D,Nmeshy);
[X,Y] = meshgrid(x,y);

% Channel
xI = linspace(L1l,L1r,Nmeshx);
yI = linspace(D,D1,Nmeshy);
[XI,YI] = meshgrid(xI,yI);

% Eigenvalues (basin; inlet channel)
lambda = @(n) sqrt((n*pi/L)^2 - K);
lambdaI = @(n) sqrt((n*pi/deltaL1)^2 - K1);

% Collocation matrix coefficient parts
beta = @(n) 1 + exp(-2.*lambda(n).*D);
betaI = @(n) exp(2.*lambdaI(n).*(D - D1)) - 1;
betad = @(n) lambda(n).*(1 - exp(-2.*lambda(n).*D));
betaId = @(n) lambdaI(n).*(exp(2.*lambdaI(n).*(D - D1)) + 1);

% Collocation matrix eigenfunction parts
phi1 = @(n,x) cos(n.*pi.*x./L);
phiI = @(n,x) cos(n.*pi.*(x - L1l)./deltaL1);

% Number of 0th order basin modes
N = 99;

% Collocation points
xB = L/(N + 1).*(0.5 + 0:(N + 1))';
xC = xB(xB > L1l & xB < L1r)';

% Number of 0th order channel modes
M = numel(xC) - 1;

% (Sub)matrix construction
B1 = zeros(N + 1);
for i = 1:N + 1
    B1(:,i) = betad(i - 1).*phi1(i - 1,xB);
end

B2 = zeros(N + 1,M + 1);
for i = 1:M + 1
    B2(:,i) = -betaId(i - 1).*phiI(i - 1,xB).*(xB >= L1l & xB <= L1r);
end

B3 = zeros(M + 1,N + 1);
for i = 1:N + 1
    B3(:,i) = beta(i - 1).*phi1(i - 1,xC);
end

B4 = zeros(M + 1);
for i = 1:M + 1
    B4(:,i) = -betaI(i - 1).*phi1(i - 1,xC);
end

% Assembling matrix and solving the coefficients
```

```
Btot = [B1 B2; B3 B4];
Ztot = [zeros(N + 1,1); Z*ones(M + 1,1)];
Atot = Btot\Ztot;

% Split the basin from channel coefficients
a = Atot(1:N + 1);
aI = Atot(N + 2:end);

% Simulate system
% Basin eigenfunction
Phi = @(n) cos(n.*pi.*X./L).*(exp(lambda(n).*(Y - D)) + exp(-lambda(n).*(Y
    + D)));
Phix = @(n) -n.*pi./L.*sin(n.*pi.*X./L).*(exp(lambda(n).*(Y - D)) + exp(-
   lambda(n).*(Y + D)));
Phiy = @(n) lambda(n).*cos(n.*pi.*X./L).*(exp(lambda(n).*(Y - D)) - exp(-
   lambda(n).*(Y + D)));

% Basin 0th order construction
Zeta0 = zeros(Nmeshy,Nmeshx);
Zeta0x = zeros(Nmeshy,Nmeshx);
Zeta0y = zeros(Nmeshy,Nmeshx);
for i = 1:N + 1
    Zeta0 = Zeta0 + a(i).*Phi(i - 1);
    Zeta0x = Zeta0x + a(i).*Phix(i - 1);
    Zeta0y = Zeta0y + a(i).*Phiy(i - 1);
end

% Channel eigenfunction
PhiI = @(n) cos(n.*pi.*(XI - L1l)./deltaL1).*(exp(lambdaI(n).*(YI - 2*D1 +
    D)) - exp(-lambdaI(n).*(YI - D)));
PhiIx = @(n) -n.*pi./deltaL1.*sin(n.*pi.*(XI - L1l)./deltaL1).*(exp(
   lambdaI(n).*(YI - 2*D1 + D)) - exp(-lambdaI(n).*(YI - D)));
PhiIy = @(n) lambdaI(n).*cos(n.*pi.*(XI - L1l)./deltaL1).*(exp(lambdaI(n)
   .*(YI - 2*D1 + D)) + exp(-lambdaI(n).*(YI - D)));

% Channel 0th order construction
ZetaI0 = Z*ones(Nmeshy,Nmeshx);
ZetaI0x = zeros(Nmeshy,Nmeshx);
ZetaI0y = zeros(Nmeshy,Nmeshx);
for i = 1:M + 1
    ZetaI0 = ZetaI0 + aI(i).*PhiI(i - 1);
    ZetaI0x = ZetaI0x + aI(i).*PhiIx(i - 1);
    ZetaI0y = ZetaI0y + aI(i).*PhiIy(i - 1);
end

% figure; mesh(X,Y,real(Zeta0)); xlabel x; ylabel y;
% figure; mesh(XI,YI,real(ZetaI0)); xlabel x; ylabel y;

%% 1 order zeta

% Bathymetries
H = {0 + 0.*(cos(3.*Y./D).^2),...
    10.*(1-1./((X - L/2).^2./(2000*L) + (Y - D).^2./(5000*D) + 1)),...
    10.*(cos(3.*X./L).^2)};
```

```
% Small parameter
delta = 0.1;

% 2D eigenvalues
lambda1 = @(n,m) (n*pi/L)^2 + (m*pi/D)^2 - K;

% Basin eigenfunction
phi1 = @(n,m) cos(n*pi/L.*X).*cos(m*pi/D.*Y);
phi1x = @(n,m) -n*pi/L.*sin(n*pi/L.*X).*cos(m*pi/D.*Y);
phi1y = @(n,m) -m*pi/D.*cos(n*pi/L.*X).*sin(m*pi/D.*Y);

% Number of 1st order basin modes
N1 = 40; M1 = 40;

% Number of 1st order channel modes
NI1 = 50;

b1 = {}; b2 = {}; c1 = {}; c2 = {}; U = zeros(numel(H),1);
c = 10;

figure; hold on
for k = 1:numel(H)
    h = H{k};
    subplot(2,numel(H),k); mesh(X,Y,h); xlabel x; ylabel y; zlabel h(x,y);

    % Calculating the Helmholtz forcing term
    intermedx = (h./M0 - H0./(r.*h./H0^2 + 1i.*omega)).*Zeta0x;
    intermedy = (h./M0 - H0./(r.*h./H0^2 + 1i.*omega)).*Zeta0y;

    diffXintermedx = zeros(Nmeshy,Nmeshx);
    diffYintermedy = zeros(Nmeshy,Nmeshx);
    for j = 2:Nmeshx - 1
        for i = 2:Nmeshy - 1
            diffXintermedx(i,j) = (intermedx(i,j + 1) - intermedx(i,j - 1)
               )/(2*L/Nmeshx);
            diffYintermedy(i,j) = (intermedy(i + 1,j) - intermedy(i - 1,j)
               )/(2*D/Nmeshy);
        end
    end

    A = M0/H0.*(diffXintermedx + diffYintermedy);

    % Coefficients through integration
    b = @(n,m) (m ~= 0 || n ~= 0).*4./(lambda1(n,m).*L.*D).*trapz(x,trapz(
       y,A.*phi1(n,m)));

    % Basin 1st order construction
    Zeta1 = zeros(Nmeshy,Nmeshx);
    Zeta1x = zeros(Nmeshy,Nmeshx);
    Zeta1y = zeros(Nmeshy,Nmeshx);
    for i = 0:N1 - 1
        for j = 0:M1 - 1
            Zeta1 = Zeta1 + b(i,j).*phi1(i,j);
```

```
            Zeta1x = Zeta1x + b(i,j).*phi1x(i,j);
            Zeta1y = Zeta1y + b(i,j).*phi1y(i,j);
        end
    end

    % M-term
    M = r./(H0 + delta.*h) - 1i.*omega;

    % First order basin flow velocities
    u = -g./M.*(Zeta0x + delta.*Zeta1x);
    v = -g./M.*(Zeta0y + delta.*Zeta1y);
    c1{k} = u;
    c2{k} = v;

%     subplot(2,numel(H),k); quiver(X(1:c:end,1:c:end),Y(1:c:end,1:c:end),
   real(u(1:c:end,1:c:end)),real(v(1:c:end,1:c:end)),'AutoScaleFactor',1);
    axis tight;

    % Coefficients through integration
    Zeta1yatD = Zeta1y(end - 1,:);
    xIint = linspace(min(xC),max(xC),Nmeshx);
    aI1 = @(n) (n ~= 0).*2/(deltaL1.*betaId(n))*trapz(xIint,Zeta1yatD.*cos
       (n.*pi.*(xIint - L1l)./deltaL1));

    % Channel 1st order construction
    ZetaI1 = zeros(Nmeshy,Nmeshx);
    ZetaI1x = zeros(Nmeshy,Nmeshx);
    ZetaI1y = zeros(Nmeshy,Nmeshx);
    for i = 0:NI1 - 1
        ZetaI1 = ZetaI1 + aI1(i).*PhiI(i);
        ZetaI1x = ZetaI1x + aI1(i).*PhiIx(i);
        ZetaI1y = ZetaI1y + aI1(i).*PhiIy(i);
    end

    % First order channel flow velocities
    uI = -g./M.*(ZetaI0x + delta.*ZetaI1x);
    vI = -g./M.*(ZetaI0y + delta.*ZetaI1y);
    b1{k} = uI;
    b2{k} = vI;

    subplot(2,numel(H),k + numel(H)); quiver(XI(1:c:end,1:c:end),YI(1:c:
       end,1:c:end),real(b1{k}(1:c:end,1:c:end)),real(b2{k}(1:c:end,1:c:
       end)),'AutoScaleFactor',1); axis tight;
    xlabel x; ylabel y;

    % Calculate mean flow speed in channel
    U(k) = mean2(abs(uI));
end
```

References

[1] Ronald L. Brouwer, Henk M. Schuttelaars, Pieter C. Roos (2013). "Modelling the influence of spatially varying hydrodynamics on the cross-sectional stability of double inlet systems". *Ocean Dynamics, 2013*(63), 1263-1278.

[2] Pieter C. Roos, Henk M. Schuttelaars, Ronald L. Brouwer (2013). "Observations of barrier island length explained using an exploratory morphodynamic model". *Geophysical Research Letters, 2013*(40), 4338–4343.

[3] R. Haberman, "Applied Partial Differential Equations with Fourier Series and Boundary Value Problems", *Pearson Education, Inc., Fifth Edition, 2013.*

[4] H. Segur, H. Yamamoto (2009). "The Shallow-Water Equations". Retrieved from https://www.whoi.edu/fileserver.do?id=136564&pt=10&p=85713

[5] P. Broomans (2003). "Numerical Accuracy in Solutions of the Shallow-Water Equations". Retrieved from http://ta.twi.tudelft.nl/users/vuik/numanal/broomans_afst.pdf

[6] MATLAB 8.6, The MathWorks Inc., Natick, MA, USA.

[7] Retrieved from https://nl.wikipedia.org/wiki/Waddenzee

[8] Retrieved from https://nl.wikipedia.org/wiki/Waddeneilanden

[9] Retrieved from http://www.waddensea-worldheritage.org/wadden-sea-world-heritage